RAD51 D-loop structures reveal the mechanism of eukaryotic RAD51-mediated strand exchange

Shih-Chi Luo[1], Cheng-Han Yang[1,2], Hsin-Yi Yeh[3], Cheng-Wei Lin[3], Min-Chi Yeh[1], Peter Chi[3] & Meng-Chiao Ho[1,3,4]

[1]Institute of Biological Chemistry, Academia Sinica, Taipei, Taiwan

[2]Institute of Oral Medicine, National Cheng Kung University, Tainan, Taiwan

[3]Institute of Biochemical Sciences, National Taiwan University, Taipei, Taiwan

[4]Graduate Institute of Biochemistry and Molecular Biology, National Taiwan University, Taipei, Taiwan.

Electronic address: joeho@as.edu.tw.

Supplementary Figures

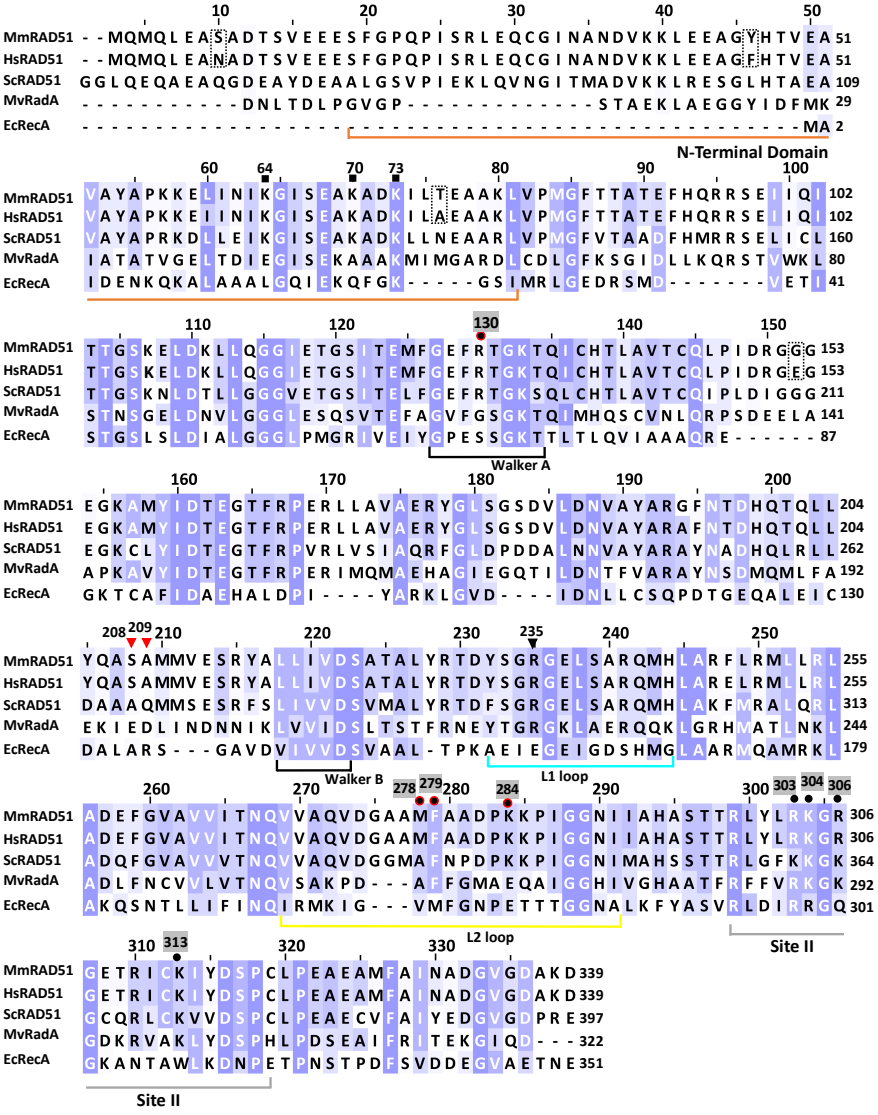

Figure S1. Multiple sequence alignment of human RAD51, mouse RAD51, and their orthologs.

The conserved Loops L1 and L2, responsible for ssDNA binding, are labeled. In the conserved N-terminal domain, residues K64, K70, and K73 for dsDNA duplex interaction are indicated with black squares. Key residues involved in contacting the displaced strand DNA within the D-loop (R130, R303, K304, R306, K313, and M278/F279) are indicated as black dots. Notably, R130, K284, M278, and F279 (black dot with red circle) are not located in the site II region. Residue R235, which interacts with the complementary strand, is marked with a black triangle. The four mutational sites differing between hRAD51 and mRAD51 (N10S, F46Y, A76T, and E152G) are highlighted with black dashed squares. The S208E and A209D mutations used to create our cryo-EM mini filament are indicated by a red triangle.

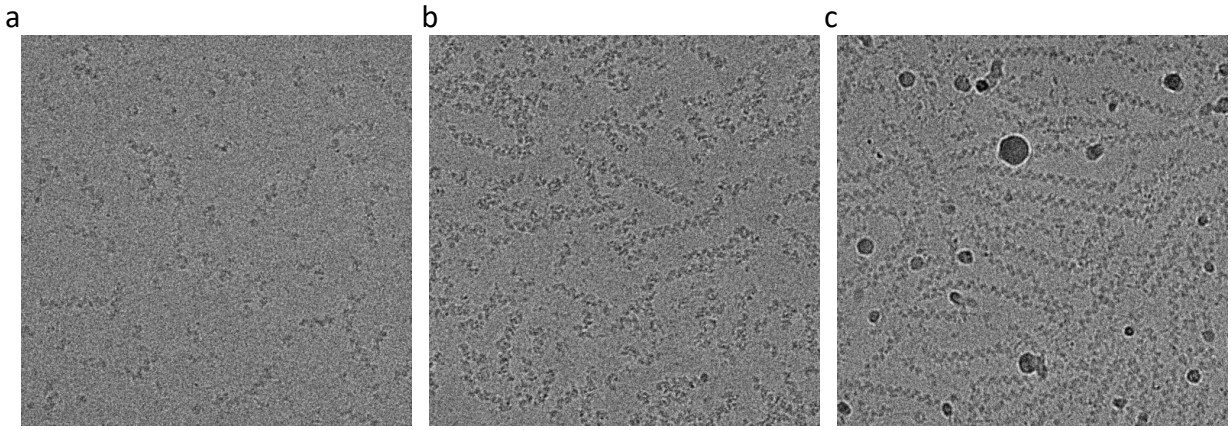

Figure S2. Time-dependent growth of RAD51-SEAD mutant filaments.
RAD51-SEAD double mutant forms progressively longer filaments with increasing incubation time. **(a)** Short incubation (~1.5 min): predominantly minifilaments. **(b)** Intermediate incubation (~3.5 min): a mixture of minifilaments and regular-length filaments. **(c)** Long incubation (~5.5 min): primarily regular-length filaments.

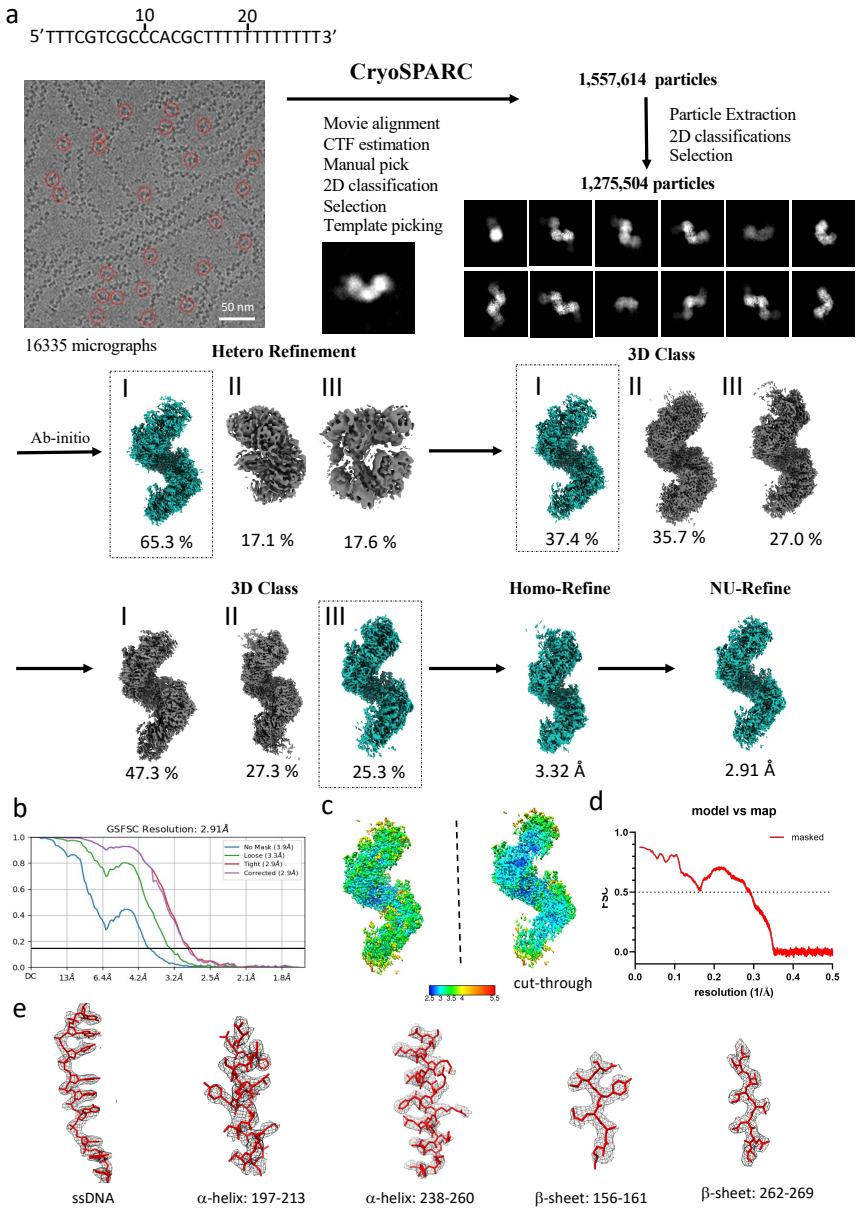

Figure S3. Cryo-EM workflow and structure determination of RAD51 presynaptic minifilament.

(a) Flowchart outlining the cryo-EM data processing and 3D reconstruction pipeline for the RAD51 presynaptic minifilament. A representative cryo-EM micrograph and 2D class average are shown at the top. Representative *ab initio* reconstructions and final refinement maps are shown below. The sequences of ssDNA for this complex is shown on top. **(b)** Gold-standard Fourier shell correlation (FSC) curves of the final 3D reconstruction. **(c)** Cryo-EM map of the RAD51 presynaptic minifilament, colored according to local resolution. **(d)** FSC curves comparing the refined atomic model with the masked map, calculated using Phenix. **(e)** Representative regions of the cryo-EM density map superimposed with the refined atomic model.

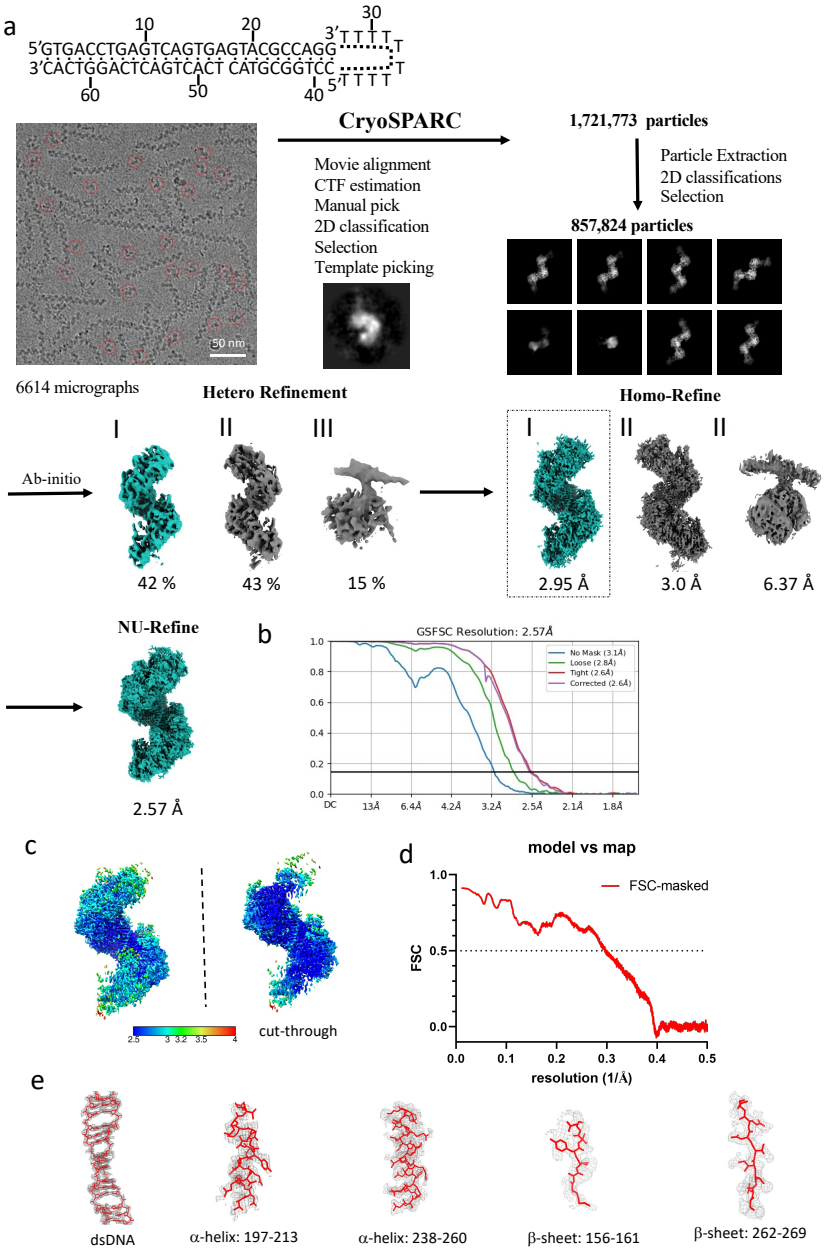

Figure S4. Cryo-EM workflow and structure determination of RAD51 postsynaptic minifilament.

(a) Flowchart outlining the cryo-EM data processing and 3D reconstruction pipeline for the RAD51 postsynaptic minifilament. A representative cryo-EM micrograph and 2D class average are shown at the top. Representative *ab initio* reconstructions and final refinement maps are shown below. The sequences of hairpin DNA for this complex is shown on top. **(b)** Gold-standard Fourier shell correlation (FSC) curves of the final 3D reconstruction. **(c)** Cryo-EM map of the RAD51 postsynaptic minifilament, colored according to local resolution. **(d)** FSC curves comparing the refined atomic model with the masked map, calculated using Phenix. **(e)** Representative regions of the cryo-EM density map superimposed with the refined atomic model.

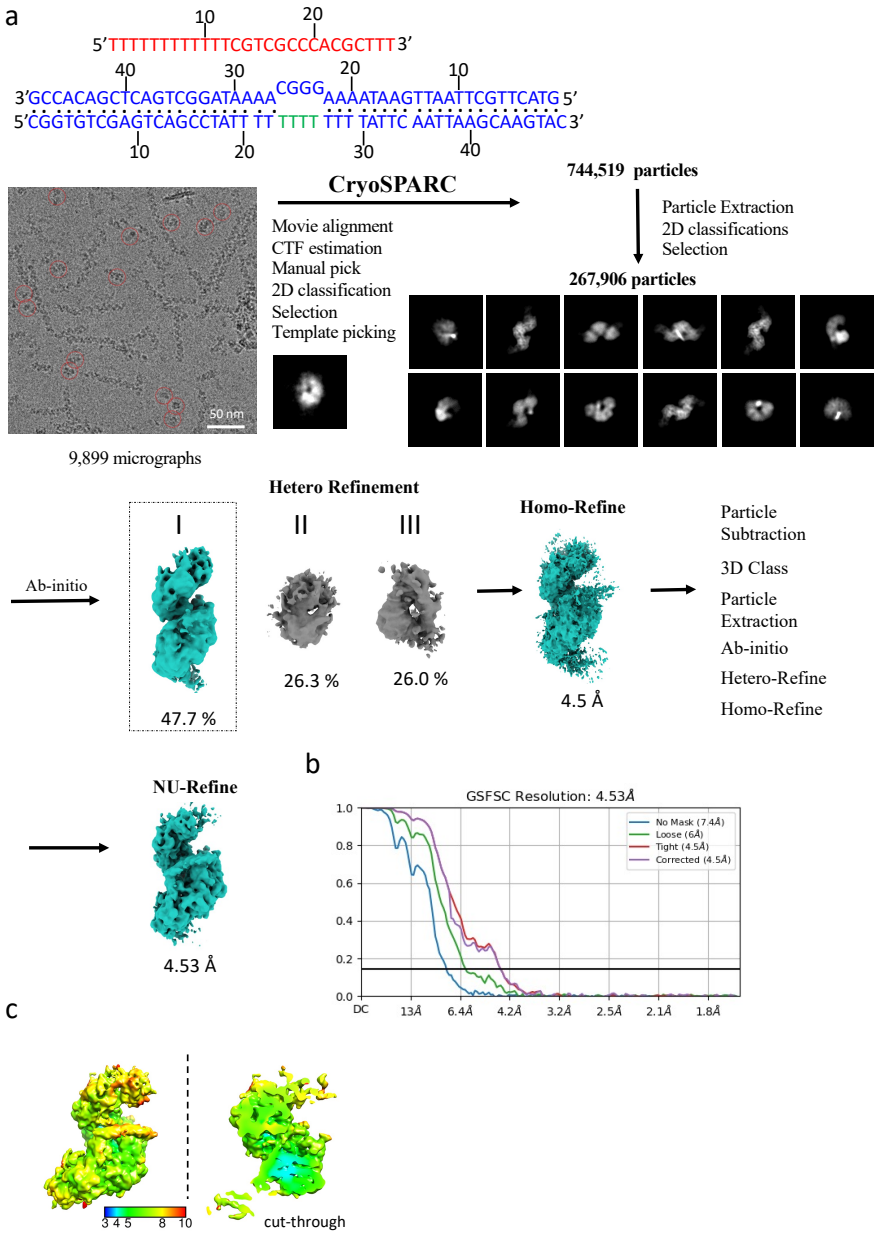

Figure S5. Cryo-EM workflow and structure determination of RAD51 minifilament complex with dsDNA at the initial recruitment state shown in figure 2a.

(a) Flowchart outlining the cryo-EM data processing and 3D reconstruction pipeline for the RAD51 minifilament with dsDNA. A representative cryo-EM micrograph and 2D class average are shown at the top. Representative *ab initio* reconstructions and final refinement maps are shown below. The sequence of ssDNA (red) and the dsDNA bubble (blue) for this complex is shown on the top. **(b)** Gold-standard Fourier shell correlation (FSC) curves of the final 3D reconstruction. **(c)** Cryo-EM map of the RAD51 inifilament, colored according to local resolution.

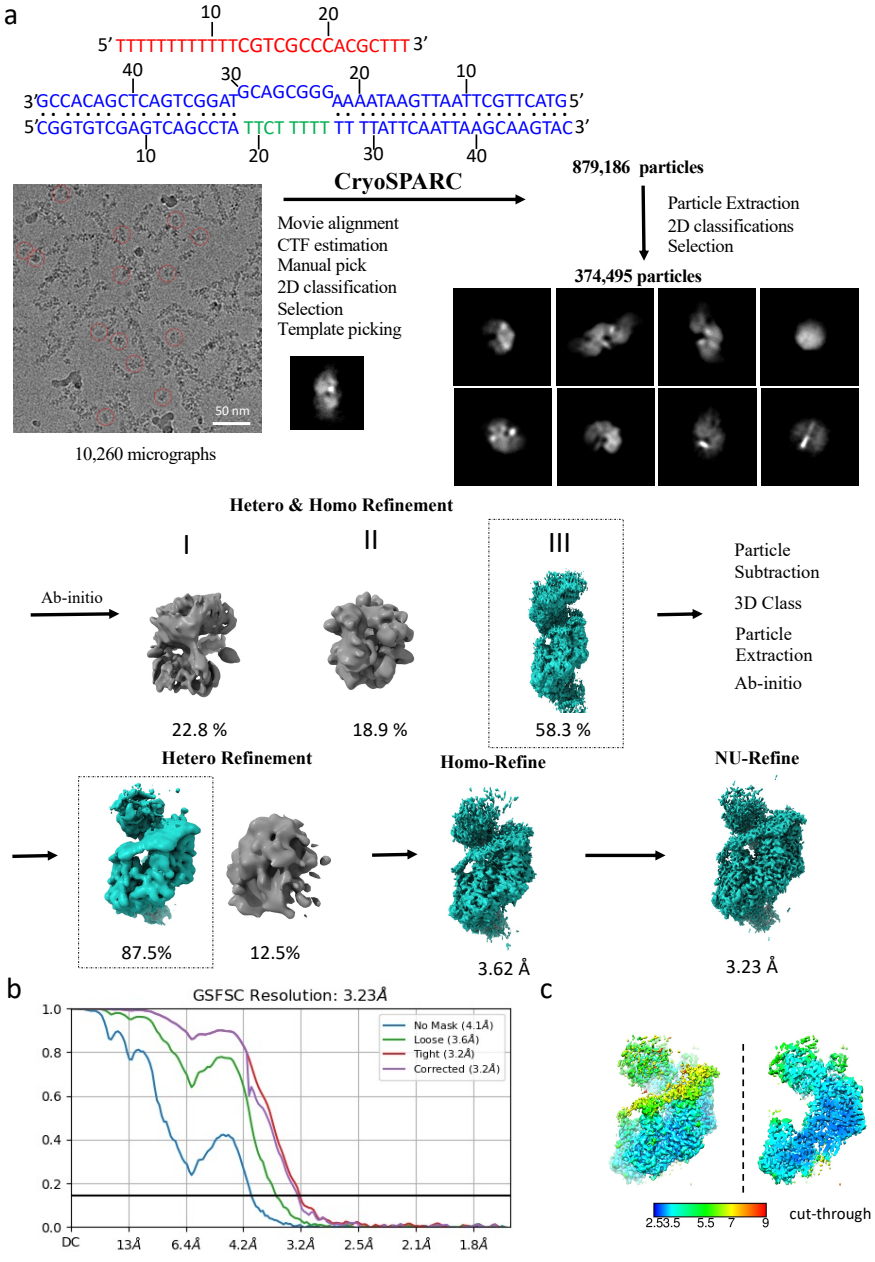

Figure S6. Cryo-EM workflow and structure determination of RAD51 minifilament complex with dsDNA after the initial recruitment state shown in figure 2b.
(a) Flowchart outlining the cryo-EM data processing and 3D reconstruction pipeline for the RAD51 minifilament with dsDNA. A representative cryo-EM micrograph and 2D class average are shown at the top. Representative *ab initio* reconstructions and final refinement maps are shown below. The sequence of ssDNA (red) and the dsDNA bubble (blue) for this complex is shown on the top. **(b)** Gold-standard Fourier shell correlation (FSC) curves of the final 3D reconstruction. **(c)** Cryo-EM map of the RAD51 minifilament, colored according to local resolution.

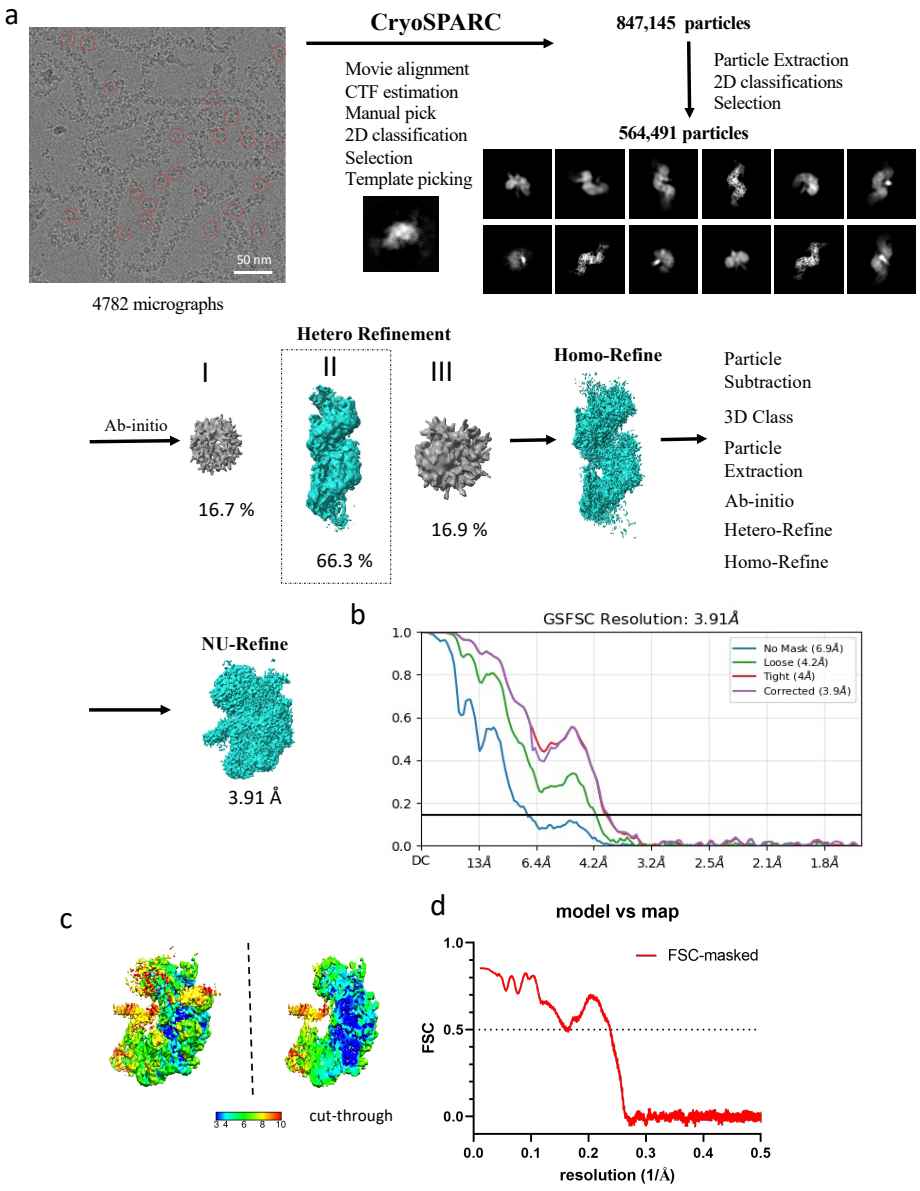

Figure S7. Cryo-EM workflow and structure determination of RAD51 D-loop shown in figure 2c and 3a-e.

(a) Flowchart outlining the cryo-EM data processing and 3D reconstruction pipeline for the RAD51 D-loop shown in figure 2c and 3a-e. A representative cryo-EM micrograph and 2D class average are shown at the top. Representative *ab initio* reconstructions and final refinement maps are shown below. **(b)** Gold-standard Fourier shell correlation (FSC) curves of the final 3D reconstruction. **(c)** Cryo-EM map of the RAD51 D-loop, colored according to local resolution. **(d)** FSC curves comparing the refined atomic model with the masked map, calculated using Phenix.

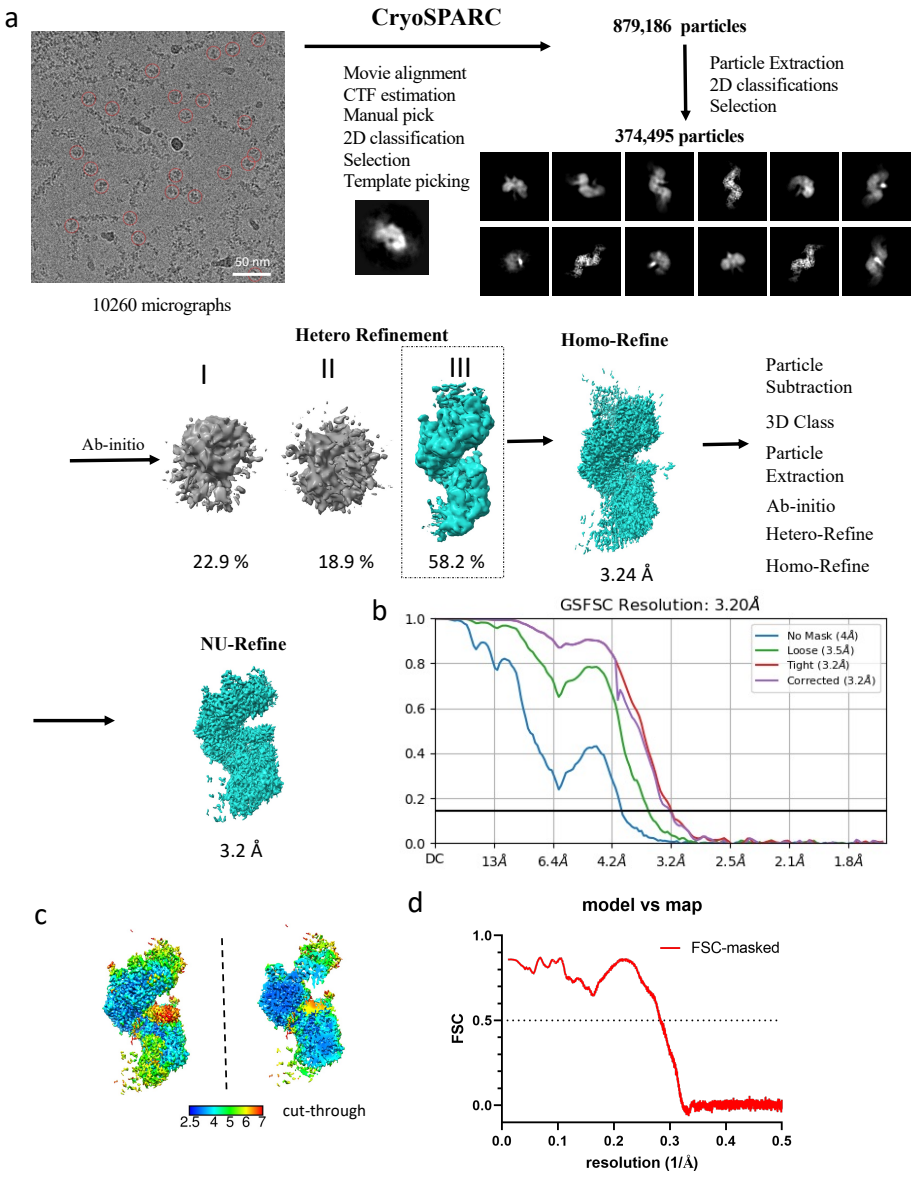

Figure S8. Cryo-EM workflow and structure determination of RAD51 D-loop shown in figure 2d and 3f-i.

(a) Flowchart outlining the cryo-EM data processing and 3D reconstruction pipeline for the RAD51 D-loop shown in figure 2d and 3f-i. A representative cryo-EM micrograph and 2D class average are shown at the top. Representative *ab initio* reconstructions and final refinement maps are shown below. **(b)** Gold-standard Fourier shell correlation (FSC) curves of the final 3D reconstruction. **(c)** Cryo-EM map of the RAD51 D-loop, colored according to local resolution. **(d)** FSC curves comparing the refined atomic model with the masked map, calculated using Phenix.

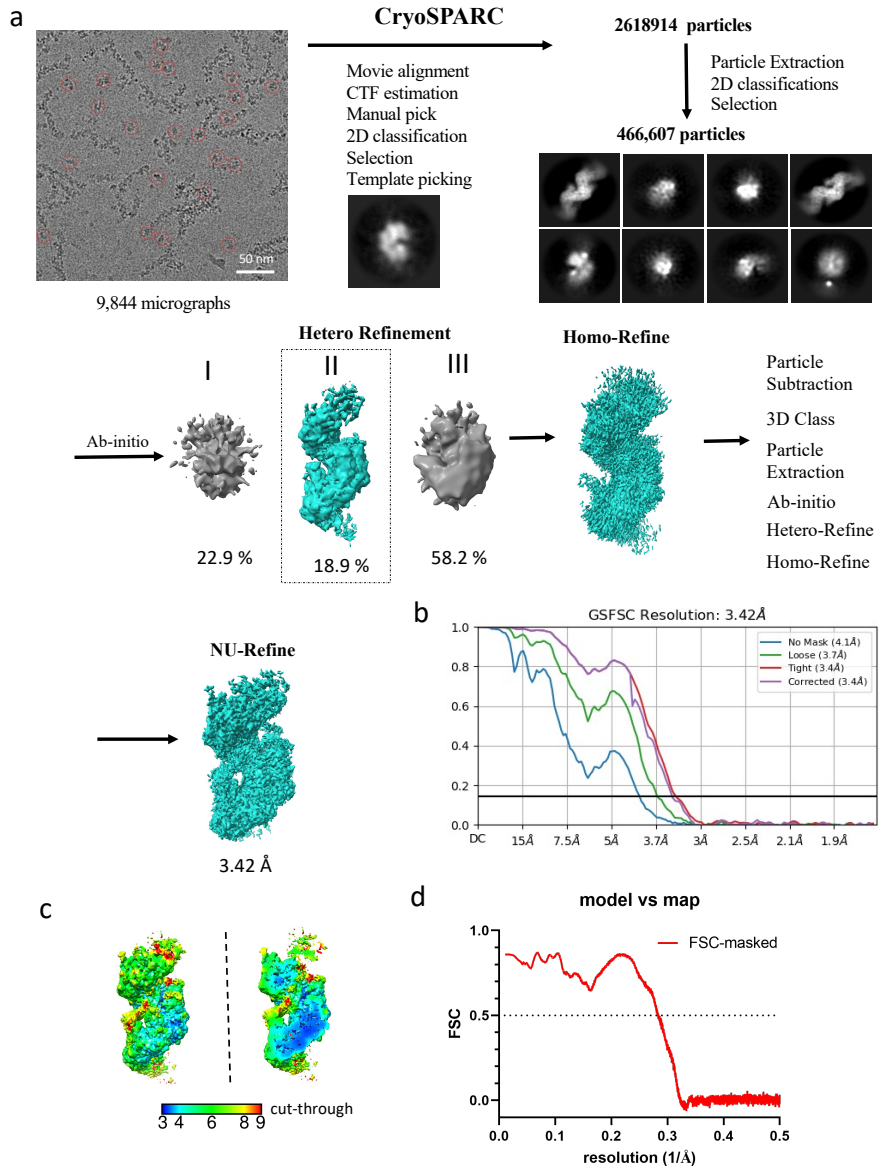

Figure S9. Cryo-EM workflow and structure determination of RAD51 D-loop shown in figure 2e and 3j-m.

(a) Flowchart outlining the cryo-EM data processing and 3D reconstruction pipeline for the RAD51 D-loop shown in figure 2e and 3j-m. A representative cryo-EM micrograph and 2D class average are shown at the top. Representative *ab initio* reconstructions and final refinement maps are shown below. **(b)** Gold-standard Fourier shell correlation (FSC) curves of the final 3D reconstruction. **(c)** Cryo-EM map of the RAD51 D-loop, colored according to local resolution. **(d)** FSC curves comparing the refined atomic model with the masked map, calculated using Phenix.

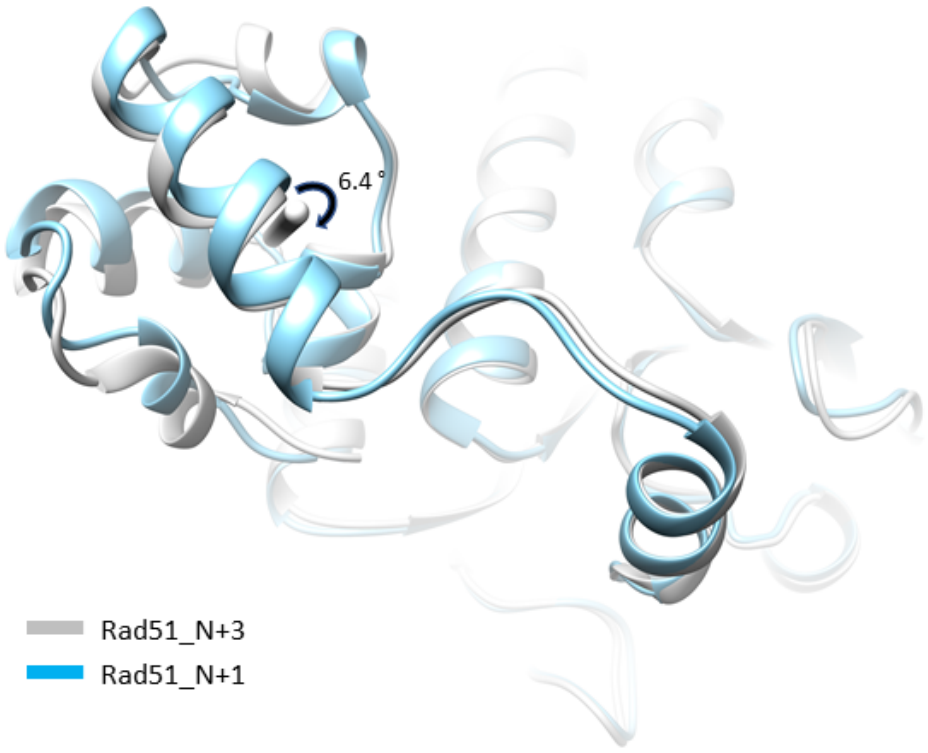

Figure S10. The NTD^{N+1} undergoes a rotation relative to RAD51^{N+3} upon D-loop formation. Superimposition of the ATPase domains of RAD51^{N+1} with RAD51^{N+3} reveals a 6.4° rotation of NTD^{N+3} around an axis near Thr76.

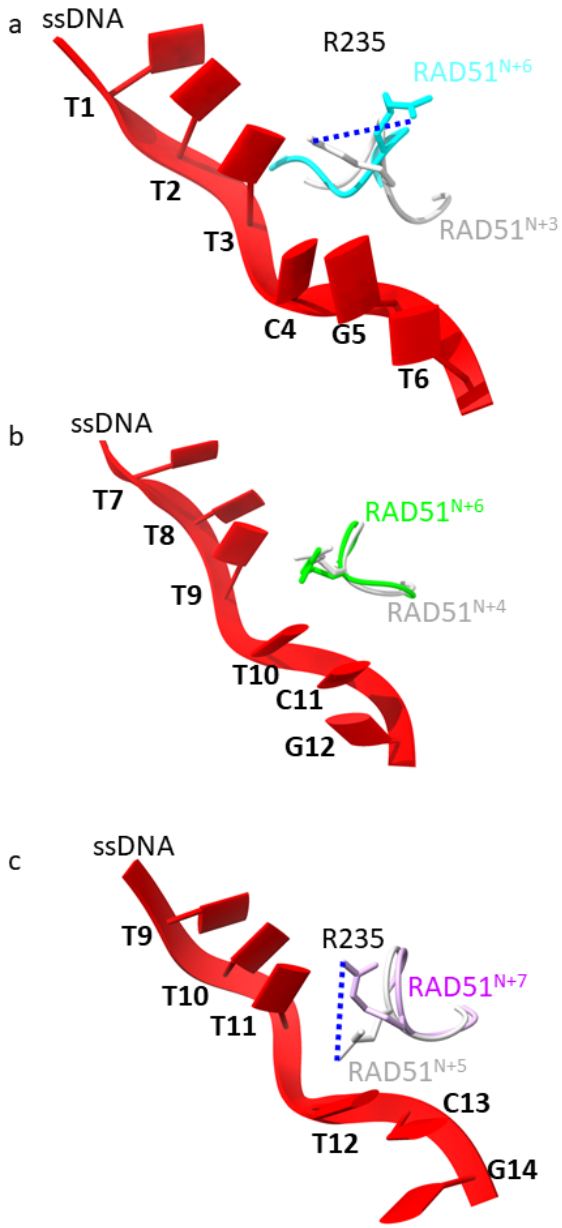

Figure S11. Comparison of Arg235 conformations in different RAD51 protomers relative to the invading DNA strand.

The invading strand is depicted in red, while Arg235 residues inserted into the inter-triplet gaps are shown in gray. The distance difference is indicated.**(a)** D-loop complex from Fig. 2c, with Arg235 adjacent to the just-separated complementary strand, colored in cyan.**(b)** D-loop complex from Fig. 2d, Arg235 positioned near the just-separated complementary strand, colored in green.**(c)** D-loop complex from Fig. 2e, Arg235 located near the just-separated complementary strand, colored in pink.

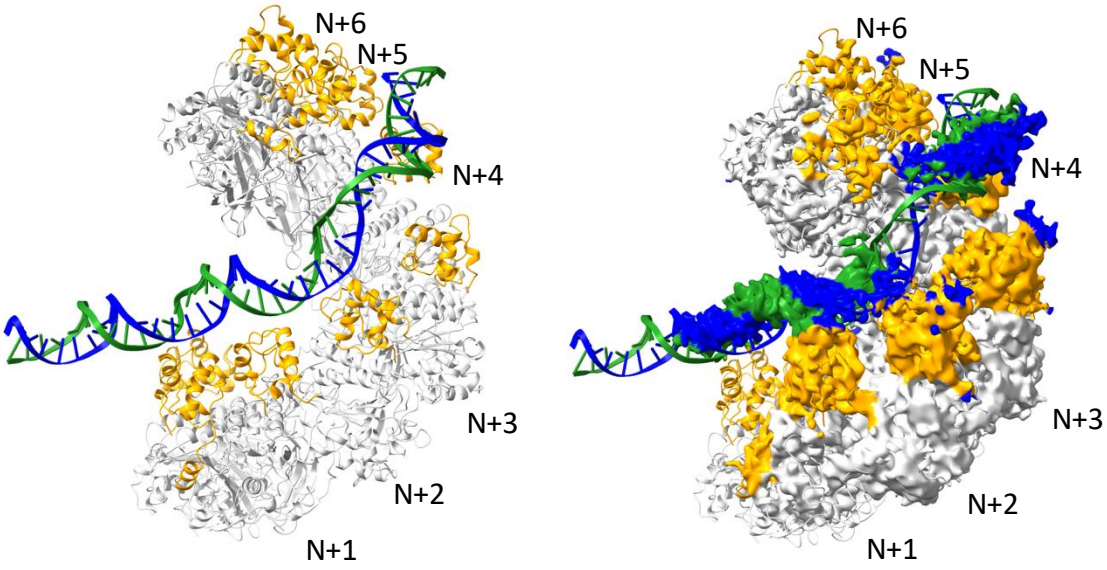

Figure. S12 Docking of molecular dynamics model into the cryo-EM map of the RAD51 D-loop complex.

The model (shown on the left) extracted from the MD simulation trajectory of D-loop initiation fits well into the experimental cryo-EM map shown in Fig. 2c (shown on the right).

Supplementary Table S1 DNA oligonucleotides used in this study

Oligo No.	Sequence
Oligo1 ssDNA	Cy5-5'AAATCAATCTAAAGTATATATGAGTAAACTTGGTCTGACAGTTACCAATGCTTAATCAGTGAGGCACCTATCTCAGCGATCTGTCTATTT-3'
Oligo2 ssDNA (+)	5'TTATGTTCATTTTTTATATCCTTTACTTTATTTTCTCTGTTTATTCATTTACTTATTTTGTATTATCCTTATCTTATTTA-3'
Oligo3 dsDNA (-)	Cy5-5'TAATACAAAATAAGTAAATGAATAAACAGAGAAAATAAAG-3'
Oligo4 dsDNA (+)	5'CTTTATTTTCTCTGTTTATTCATTTACTTATTTTGTATTA-3'

Table S2. Cryo-EM data collection, refinement and validation statistics

	#1 presynaptic (EMDB-64183) (PDB 9UI4)	#2 postsynaptic (EMDB-64184) (PDB 9UI5)	#3 4 base-pair D-loop (EMDB-64186) (PDB 9UI7)
Data collection and processing			
Magnification	105,000	105,000	105,000
Voltage (kV)	300	300	300
Electron exposure (e–/Å^2)	50	50	50
Defocus range (μm)	-1.0 to -1.6	-1.0 to -1.6	-1.0 to -1.6
Pixel size (Å)	0.83	0.83	0.83
Symmetry imposed	C1	C1	C1
Final particle images (no.)	67,329	361,017	14,688
Box size (pixel)	384	384	384
Map resolution (Å)	2.91	2.57	3.91
FSC threshold	0.143	0.143	0.143
Map resolution range (Å)	2.47-7.16	1.81-5.55	3.39-10.44
Refinement			
Initial model used (PDB code)	5H1B	5H1C	7JY9
Model resolution (Masked, Å)	3.4	3.4	4.1
FSC threshold	0.5	0.5	0.5
Map sharpening *B* factor (Å^2)	-70.7	-88.4	-87.1
Model composition			
Non-hydrogen atoms	22,086	22,841	18,645
Protein residues	2,760	2,807	2187
Nucleotide	9	9	7
Ligands: ADP	9	9	7
B factors (Å^2)			
Protein	82.63	141.20	135.07
Nucleic acid	64.43	106.98	299.01
Ligand	74.0	123.45	131.32
R.m.s. deviations			
Bond lengths (Å)	0.008	0.003	0.009
Bond angles (°)	1.269	0.860	1.347
Validation			
MolProbity score	3.19	2.96	2.05
Clash score	17.59	19.23	11.88
Poor rotamers (%)	13.99	5.68	0.80
Ramachandran plot			
Favored (%)	88.95	87.7	92.75
Allowed (%)	10.06	11.43	6.78
Disallowed (%)	0.99	0.86	0.46

Table S3. Continued Cryo-EM data collection, refinement and validation statistics

	#4 8 base-pair D-loop (EMDB-64187) (PDB 9UI8)	#5 12 base-pair D-loop (EMDB-64188) (PDB 9UI9)
Data collection and processing		
Magnification	105,000	105,000
Voltage (kV)	300	300
Electron exposure (e–/Å^2)	50	50
Defocus range (μm)	-1.0 to -1.6	-1.0 to -1.6
Pixel size (Å)	0.83	0.83
Symmetry imposed	C1	C1
Total particle images (no.)	53,493	45,865
Box size (pixel)	384	
Map resolution (Å)	3.2	3.42
FSC threshold	0.143	0.143
Map resolution range (Å)	2.84-8.09	2.99-8.83
Refinement		
Initial model used (PDB code)	7JY9	7JY7
Model resolution (Masked, Å)	3.4	3.6
FSC threshold	0.5	0.5
Map sharpening *B* factor (Å^2)	-91.5	-83.9
Model composition		
Non-hydrogen atoms	23,041	23613
Protein residues	2,792	2807
Nucleotide	9	9
Ligands: ADP	9	9
B factors (Å^2)		
Protein	130.84	128.38
Nucleic acid	154.12	244.66
Ligand	121.9	97.82
R.m.s. deviations		
Bond lengths (Å)	0.005	0.008
Bond angles (°)	0.966	1.185
Validation		
MolProbity score	3.19	3.07
Clash score	20.08	15.66
Poor rotamers (%)	12.27	11.75
Ramachandran plot		
Favored (%)	89.38	89.75
Allowed (%)	10.33	9.82
Disallowed (%)	0.29	0.43